Temperature and $K\alpha$-yield radial distributions in laser-produced solid-density plasmas imaged with ultrahigh-resolution x-ray spectroscopy

U. Zastrau,[1,*] P. Audebert,[2] V. Bernshtam,[3] E. Brambrink,[2] T. Kämpfer,[1] E. Kroupp,[3] R. Loetzsch,[1] Y. Maron,[3] Yu. Ralchenko,[4] H. Reinholz,[5] G. Röpke,[5] A. Sengebusch,[5] E. Stambulchik,[3] I. Uschmann,[1] L. Weingarten,[3] and E. Förster[1]

[1]*Institut für Optik und Quantenelektronik, Friedrich-Schiller-Universität, Max-Wien-Platz 1, 07743 Jena, Germany*

[2]*Laboratoire pour l'Utilisation des Lasers Intenses, UMR 7605 CNRS-CEA, Ecole Polytechnique, Palaiseau, France*

[3]*Faculty of Physics, Weizmann Institute of Science, Rehovot 76100, Israel*

[4]*National Institute of Standards and Technology, Gaithersburg, Maryland 20899-8422, USA*

[5]*Institut für Physik, Universität Rostock, Universitätsplatz 3, 18051 Rostock, Germany*

We study warm dense matter formed by subpicosecond laser irradiation at several 10^{19} W/cm^2 of thin Ti foils using x-ray spectroscopy with high spectral ($E/\Delta E \sim 15,000$) and one-dimensional spatial ($\Delta x = 13.5$ μm) resolutions. Ti $K\alpha$ doublets modeled by line-shape calculations are compared with Abel-inverted single-pulse experimental spectra and provide radial distributions of the bulk-electron temperature and the absolute-photon number $K\alpha$ yield in the target interiors. A core with ~ 40 eV extends homogeneously up to ten times the laser-focus size. The spatial distributions of the bulk-electron temperature and $K\alpha$ yield are strongly correlated.

The generation of strongly coupled plasmas gains increasing interest for studying matter with properties between cold condensed materials and hot dense plasmas. This so-called warm dense matter (WDM) [1] is of paramount importance for modeling astrophysical objects. It occurs as a transient state in novel experiments generating high-energy plasma in materials and is of particular importance for the success of inertial confinement fusion [2]. A proper description of strongly coupled plasmas formed by relativistic laser-matter interaction is needed for the fast ignitor scheme [3] in laser-fusion research. Further, it enables progress in key applications including laser-driven x-ray sources [4], which can be used, e.g., in backlighting [5], e.g., for x-ray Thomson scattering experiments [6], or can provide alternative radiation sources for both scientific and medical applications.

To achieve highest intensities, a laser pulse is focused to diameters of a few micrometers, where lateral gradients of the generated-plasma parameters are expected to be of a similar scale. Thus, in order to achieve precise knowledge on the physical properties, such as the plasma temperature at solid density, high spatial resolution is needed [7,8]. For example, it was reported that the plasma temperature depends on the irradiated foil thickness [9,10] and is a function of depth [11]; however, no evidence of radial variations of the plasma properties has yet been experimentally obtained at solid density, while such variations could be crucial for many applications.

Short-pulse ($\lesssim 1$ ps) high-power ($\gtrsim 10^{19}$ W/cm^2) laser interaction with solid targets is a highly complex issue. A thin hot plasma layer formed at the surface of the target supplies electrons that are accelerated and pushed through the cold solid bulk material, mainly by the ponderomotive forces [12]. These fast electrons reach relativistic energies with a Maxwellian-like distribution [13]. The most energetic electrons leave the foil rear side [14], while electrons with lower energies deposit their entire energy inside the foil. The energetic electrons traversing the target produce K-shell vacancies, leading to the characteristic inner-shell emission. The process is further complicated by prepulses that for such high-power lasers could reach intensities above 10^{12} W/cm^2, and therefore preionize the target. In a nanosecond before the arrival of the main pulse, the plasma expands and the sharp target-vacuum boundary changes into a density gradient [15], resulting in a significant scatter of the results obtained in seemingly similar experiments.

Measurements of the characteristic $K\alpha$ emission have proven to be reliable diagnostics for solid-state-density plasmas. First, the plasma parameters strongly affect the structure of the emitted lines. In particular, the emerge of the blue satellites due to the formation of M-shell holes is an indicator for the bulk-electron temperature [9]. Second, solid-density plasma is transparent to the emitted x-rays, which, therefore, yield unique information on the target interior. This is a large advantage over measurements of XUV or visible radiation. The latter could be employed to probe only the surface plasma, e.g., [16]. Moreover, the x-ray emission occurs within a few picoseconds, well below the typical hydrodynamic expansion time [4,17,18].

In this paper we report on radially resolved distributions of the bulk-electron temperature and absolute $K\alpha$ yield in laser-produced WDM. This was achieved by employing high-resolution one-dimensional (1D) imaged x-ray spectroscopy of the Ti $K\alpha$ doublet, with a spatial resolution comparable to the laser focal size. The electron-temperature radial distributions were reconstructed using line-shape modeling of the Abel-inverted laterally imaged Ti $K\alpha$ doublet. Furthermore, in order to probe the influence of the prepulse, we also performed measurements with increased laser contrast ratio obtained by frequency doubling. For the measurements, foils with various thicknesses, as well as a bulk target, were used.
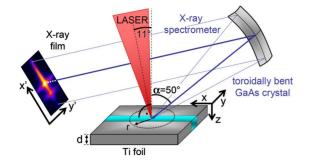
*ulf.zastrau@uni-jena.de

FIG. 1. (Color online) Schematic of the experimental setup. The energy dispersion axis x' on the x-ray film is perpendicular to the spatial resolution in the y direction.
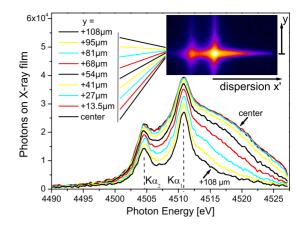

FIG. 2. (Color online) Single-pulse x-ray spectra of the laser-irradiated 10-μm-thick Ti foil at laser intensity $I = 5 \times 10^{19}$ W/cm^2 and $\lambda = 1057$ nm, shown from different target positions y. The x-ray film scan (false colors) is given in the inset.

The experiments were performed at the *LULI 100TW* laser facility [19]. In our experiments, the maximum energy on target is about 14 J with a pulse duration of 330 fs. The laser pulse is focused by a parabolic mirror to focal spot sizes down to 8 μm in diameter, yielding intensities $(5 \pm 1) \times 10^{19}$ W/cm^2 at the fundamental wavelength $\lambda = 1057$ nm. Amplified spontaneous emission and prepulses within the first nanosecond before the main pulse have a contrast ratio of 10^{-8}. When the laser pulse is frequency doubled ($\lambda = 529$ nm), the intensity is $(2 \pm 1) \times 10^{19}$ W/cm^2 and the contrast ratio is increased to 10^{-10} [20]. The incidence angle to the target normal was $11°$ (Fig. 1). The laser pulse is p polarized at the fundamental frequency (ω) and s polarized at the frequency-doubled mode (2ω), respectively. For the targets, 25-, 10-, and 5-μm-thick Ti foils, as well as Ti bulk, were used. The 5 μm foil was coated by 250 nm of copper, to eliminate the Ti $K\alpha$ radiation from the hot plasma at the surface of the foil.

Time-integrated single-pulse spectra of the $K\alpha$-doublet emission (4490–4530 eV) are detected using a toroidally bent GaAs crystal x-ray spectrometer [21] with radii of 450 mm in the sagittal direction and 306 mm in the meridional direction. The plasma is located inside the Rowland circle and is imaged with a magnification of 1.8. An x-ray film was placed along the Rowland circle. The y axis is inferred from y' by applying the magnification, while x' refers to the dispersion axis, as illustrated in Fig. 1.

The measured spectrum $I_M(x', y)$ as a function of the coordinates x' and y (as shown in Fig. 1) is the local emissivity $I(E, r, z)$ integrated along both the x axis and the target depth z, as indicated by the highlighted slice in Fig. 1, where conversion from x' to E is obtained by applying a nonlinear dispersion relation [21]. Thus,

$$I_M(E, y) = \int_0^d dz \int_{-\infty}^{+\infty} dx I(E, r, z) w(E, r, z), \quad (1)$$

where d is the target thickness and $r = (x^2 + y^2)^{1/2}$. We assume axial symmetry of the $K\alpha$ emission, with the axis perpendicular to the target surface. $w(E, r, z)$ is the attenuation factor due to the attenuation length ℓ inside the target,

$$w(E, r, z) = \exp\left\{-\int_0^z \frac{dz'}{\ell(E, r, z') \cos \alpha}\right\}. \quad (2)$$

Here, $\alpha = 50°$ is the angle between the observation direction and the normal to the target (see Fig. 1).

The spectral resolution was determined to be $E/\Delta E \geq 15\,000$, limited by the measured rocking curve and independent of the plasma size due to the use of the Johann scheme [22]. The spatial resolution in the meridional direction is 4 μm [23]. The efficiency of this spectrometer is $N_{\rm det}/N_0 = 2 \times 10^{-5}$ [21]. All spectra were recorded using Kodak Industrex x-ray film, which was absolutely calibrated by comparison to a characterized *p-i-n* x-ray diode [24]. Together with the known crystal efficiency, we are able to infer absolute-photon numbers. The films were scanned along the spatially resolved axis by means of a Zeiss densitometer with steps of $y = 13.5$ μm, yielding an optimal signal-to-noise ratio.

The bent-crystal spectrometer yields 1D resolved spectra of the plasma emission, as shown in Fig. 2. In this exposure a 5×10^{19} W/cm^2 intense laser pulse at the fundamental wavelength hit a 10 μm thin Ti foil. From the center of emission up to $y = 27$ μm, i.e., very close to the laser focus, we observe the same profile and emissivity. Then, a dramatic change in the profiles is observed with every further step of 13.5 μm. All profiles show a significant blue wing and a rather smooth profile without additional peaks, and we observe no shifted position of the $K\alpha_1$ and $K\alpha_2$ components.

We now assume that contribution of the resonant self-absorption in the plasma to ℓ is minor. Thus, we use $\ell = \ell_0 = 20$ μm of the solid-state titanium, which is practically constant over the rather narrow spectral range of interest [25]; i.e., w is solely a function of z, $w(z) = \exp[-z/(\ell_0 \cos \alpha)]$. For the thin foils, we note that d is comparable or smaller than $\ell_0 \cos \alpha$, and the attenuation is rather minor, e.g., giving $w \approx 0.5$ for photons coming from the back side of a 10 μm foil. On the other hand, spectra obtained from bulk targets represent mostly the radiation from the front-side 20-μm-thick layer.

By applying the inverse Abel transform [26] to the measured spectrum, we obtain

$$\bar{I}(E, r) = \int_0^d dz \exp\left\{-\frac{z}{\ell_0 \cos \alpha}\right\} I(E, r, z). \quad (3)$$

Thus, the Abel inversion recovers the radial dependence of the plasma emission; the spectrum inferred, however, is av-
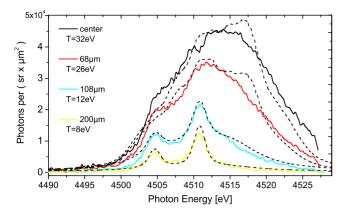
FIG. 3. (Color online) Comparison of assorted Abel-inverted experimental spectra (solid lines) from irradiation of a 10 μm Ti foil and the best-fit modeled spectra (dashed lines).
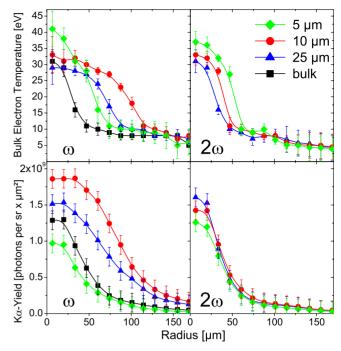

FIG. 4. (Color online) Radial temperature (top) and integrated $K\alpha$-yield (bottom) distributions of the different targets used, irradiated with the ω and 2ω laser pulses.

eraged [with the proper weight $w(z)$] over the target depth d. For each photon energy, we applied the inverse Abel transformation using the *onion-peeling* method [27], yielding radially resolved spectra in steps of 13.5 μm.

A thorough self-consistent modeling requires calculations that should account for satellite formation and blending, plasma polarization, Stark broadening, and self-absorption. Spectra of the titanium $K\alpha$ doublet were modeled using two different approaches [28,29], which yield approximately the same results. The bulk-electron temperature is the only free parameter in the modeling of the $K\alpha$ shape, assuming that the fast electrons represent a small fraction of the total electron density [28]. Except for this assumption, the fast electrons are treated in exactly the same way as the bulk electrons; i.e., they contribute to all atomic impact processes. In particular, the inner-shell-hole populations are obtained self-consistently. Thus, by varying $T_{\mathrm{e}}^{(\mathrm{bulk})}$, the total electron density, the charge-state distribution, and populations of different levels are calculated self-consistently. We use the spectra from [28] to fit the deconvoluted data in order to determine the radially resolved T_{e}. Applying this procedure for every data set, T_{e} is inferred with a 13.5 μm resolution.

Figure 3 shows a few radially resolved Ti-$K\alpha$ spectra obtained by the Abel transformation of the data presented in Fig. 2 and their best fits. At radii $\geq$120 μm we observe a narrow doublet structure, similar to those obtained from an x-ray tube. Closer to the emission center, a blue wing emerges and for radii $\leq$40 μm the fine structure is completely smeared, resulting in a broad blueshifted line profile with a full width at half maximum (FWHM) of $\approx$20 eV and an integrated emission 11$\times$ stronger than that at r =200 μm. These features are characteristic of higher bulk temperatures, with significant contributions of higher ionization stages and exited-state satellites; the Stark broadening contributes to the "smoothing" of the entire line shape. As seen in Fig. 3, a good agreement was achieved for all radii. The error bars were determined by varying T_{e} around the best-fit value (which gives a minimal χ^2) up to a 50% increase in χ^2. The line shapes do not change significantly below $T_{\mathrm{e}} \approx 5$ eV, resulting in relatively large error bars at radii $\geq$120 μm.

The radial temperature profiles and $K\alpha$ yield for both lower laser contrast (ω) and high laser contrast (2ω) are presented in Fig. 4. The maximum temperature is constantly $\sim$30–40 eV within the error bars. At ω, this temperature extends over $\sim$50 μm which is an order of magnitude larger than the laser focal spot. Its radius is increasing for thinner foils, especially for the 10 μm foil. The 5 μm foil has a smaller hot area with $r \approx 50$ μm; however, the maximum temperature exceeds 40 eV.

For the 2ω exposures, we find a more systematic dependence: both the maximum temperature and the heated area radius rise when the foil thickness decreases. The temperatures rise from 32 to 37 eV, while the radii range from 30 to 60 μm. Further, the $K\alpha$ yield decreases with thinner foils. At larger radii temperature gradients of $\sim$1 eV/μm are present.

Although some of the inferred dependences can be attributed to pulse-to-pulse laser-parameter variations, a strong correlation between the spatial distributions of $T_{\mathrm{e}}^{(\mathrm{bulk})}$ and $K\alpha$ yield is observed in each single-pulse measurement, see Fig. 5, where the FWHM values of these distributions are shown for different target thicknesses, both for ω and 2ω pulses. These results show that there is a strong correlation between the mechanism(s) responsible for the radial distribution of the electrons with $E > 5$ keV (that give rise to the $K\alpha$ radiation), and those of the WDM bulk-heating, indicating that for the latter, the faster electrons could play an important role.

The differences of the 2ω exposures compared to the ω ones are most likely related to the significantly suppressed laser-preplasma interaction due to the higher contrast ratio. Hydrodynamics simulations [20] show that for a metal foil the surface of critical electron density $n_{\mathrm{crit}} \approx 10^{21}$ cm^{-3} has moved $\approx$10 μm away from the foil as a result of the
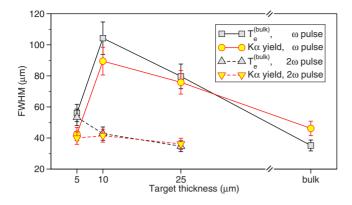
FIG. 5. (Color online) Comparison of FWHM of the bulk-electron temperature and $K\alpha$-yield radial distributions for different targets and laser pulses.

prepulse. At ω, only the 5 μm foil shows a comparatively small heated area. This may also be related to preplasma formation. As already mentioned, this foil was coated with 250 nm of copper, where the preplasma formation is likely. We note that this may also be responsible for similar radial distributions for this foil (see Fig. 5), contrary to the other targets.

It should be stressed that the higher temperatures at the center of the target, inferred using the radially resolved measurements presented here, are impossible to detect with measurements lacking spatial resolution. Indeed, a spatially integrated spectrum of the data shown in Fig. 2 is best fitted with $T_e^{(bulk)} = 10 \pm 2$ eV only, which is about *three times* lower than that at the center of the target. Evidently, such a difference could be crucial for many applications. For example, it has been shown [30] that an increase of only $\approx 20\%$ in the bulk-electron temperature could increase the neutron yield by a factor of 10–30 in the fast ignition scheme.

In conclusion, the generated plasma shows a rather homogeneous core heated to T that is several times higher than the averaged one and up to an order of magnitude larger than the laser focal spot, and surrounded by an even larger area of a colder (yet $K\alpha$-emitting) WDM, with a strong similarity between radial distributions of the bulk-electron temperature and the $K\alpha$ yield. The influence of a thin coating on the 5 μm foil results in both a decreased spot size and $K\alpha$ yield. When the laser frequency is doubled and the contrast is increased to 10^{-10}, the inferred distributions become $\sim 2\times$ narrower and show a clear dependence on the foil thickness: the generated plasma from thin foils is hotter and the yield is lower. The results are of primary importance for basic understanding of laser-matter interaction, benchmarking computer simulations, and various applications, such as laser-driven backlighters and fast ignition laser fusion. In the latter case, doping the low-Z targets with an appropriate middle-Z species is suggested.

[1] R. W. Lee *et al.*, Laser Part. Beams **20**, 527 (2002).
[2] J. D. Lindl *et al.*, Phys. Plasmas **11**, 339 (2004).
[3] M. Tabak *et al.*, Phys. Plasmas **1**, 1626 (1994).
[4] C. Reich, I. Uschmann, F. Ewald, S. Düsterer, A. Lübcke, H. Schwoerer, R. Sauerbrey, E. Förster, and P. Gibbon, Phys. Rev. E **68**, 056408 (2003).
[5] H. Park *et al.*, Rev. Sci. Instrum. **75**, 4048 (2004).
[6] O. Landen *et al.*, J. Quant. Spectrosc. Radiat. Transf. **71**, 465 (2001).
[7] A. Saemann, K. Eidmann, I. E. Golovkin, R. C. Mancini, E. Andersson, E. Förster, and K. Witte, Phys. Rev. Lett. **82**, 4843 (1999).
[8] G. Malka *et al.*, Phys. Rev. E **77**, 026408 (2008).
[9] S. Hansen *et al.*, Phys. Rev. E **72**, 036408 (2005).
[10] S. Chen *et al.*, Phys. Plasmas **16**, 062701 (2009).
[11] R. Evans *et al.*, Appl. Phys. Lett. **86**, 191505 (2005).
[12] J. Gordon, Phys. Rev. A **8**, 14 (1973).
[13] P. Gibbon *et al.*, Plasma Phys. Controlled Fusion **38**, 769 (1996).
[14] B. Hidding *et al.*, Rev. Sci. Instrum. **78**, 083301 (2007).
[15] P. Audebert, J. P. Geindre, S. Rebibo, and J. C. Gauthier, Phys. Rev. E **64**, 056412 (2001).
[16] M. Nakatsutsumi *et al.*, New J. Phys. **10**, 043046 (2008).
[17] S. Chen *et al.*, Phys. Plasmas **14**, 102701 (2007).
[18] P. Audebert, R. Shepherd, K. B. Fournier, O. Peyrusse, D. Price, R. Lee, P. Springer, J. C. Gauthier, and L. Klein, Phys. Rev. Lett. **89**, 265001 (2002).
[19] B. Wattellier *et al.*, Opt. Lett. **29**, 2494 (2004).
[20] S. Baton *et al.*, Phys. Plasmas **15**, 042706 (2008).
[21] T. Missalla *et al.*, Rev. Sci. Instrum. **70**, 1288 (1999).
[22] H. H. Johann, Z. Phys. **69**, 185 (1931).
[23] F. Zamponi *et al.*, High Energy Density Phys. **3**, 297 (2007).
[24] L. Cibik, *Calibration Certificate 67506* (Physikalisch-Technische Bundesanstalt, Germany, 2006).
[25] B. L. Henke *et al.*, At. Data Nucl. Data Tables **54**, 181 (1993).
[26] H. R. Griem, *Principles of Plasma Spectroscopy* (Cambridge University Press, Cambridge, 1997).
[27] C. Dasch, Appl. Opt. **31**, 1146 (1992).
[28] E. Stambulchik *et al.*, J. Phys. A **42**, 214056 (2009).
[29] A. Sengebusch *et al.*, J. Phys. A **42**, 214061 (2009).
[30] R. Kodama *et al.*, Nature (London) **412**, 798 (2001).